A revisit of parametrization of downward longwave radiation in summer over the Tibetan Plateau based on high temporal resolution measurements

Mengqi Liu[a,c], Xiangdong Zheng[d], Jinqiang Zhang[a,b,c] and Xiangao Xia[a,b,c]

[a] LAGEO, Institute of Atmospheric Physics, Chinese Academy of Sciences, Beijing, 100029, China

[b] Collaborative Innovation Center on Forecast and Evaluation of Meteorological Disasters, Nanjing University of Information Science & Technology, Nanjing 210044, China

[c] College of Earth and Planetary Sciences, University of Chinese Academy of Sciences, Beijing, 100049, China

[d] Chinese Academy of Meteorological Sciences, Chinese Meteorological Bureau, Beijing, 100081, China

Abstract

The Tibetan Plateau (TP) is one of research hot spots in the climate change research due to its unique geographical location and high altitude. Downward longwave radiation (DLR), as a key component in the surface energy budget, is of practical implications for radiation budget and climate change. A couple of attempts have been made to parametrize DLR over the TP based on hourly or daily measurements and crude clear sky discrimination methods. This study uses 1-minute shortwave and longwave radiation measurements at three stations over TP to parameterize DLR during summer months. Three independent methods are used to discriminate clear sky from clouds based on 1-minute radiation and Lidar measurements. This guarantees strict selection of clear sky samples that is fundamental for the parameterization of clear-sky DLR. Eleven clear-sky and four cloudy DLR parameterizations are examined and locally calibrated. Comparing to previous studies, DLR parameterizations here are shown be characterized by smaller root mean square error (RMSE) and higher coefficient of determination (R^2). Clear-sky DLR can be estimated from the best parametrization with RMSE of 3.8 $W \cdot m^{-2}$ and $R^2 > 0.98$. Systematic overestimation of clear-sky DLR by the locally calibrated parametrization in previous study is found to be approximately 25 W m^{-2} (10%), which is very likely due to potential residual cloud contamination on previous clear-sky DLR parametrization. Cloud-base height under overcast conditions is shown to play an important role in cloudy DLR parameterization, which is considered in the locally calibrated parameterization over the TP for the first time. Further studies on DLR parameterization during nighttime and in seasons except summer are required for our better understanding of DLR's role in climate change based on 1-minute high-quality DLR measurements.

1 Introduction

The downward longwave radiation (DLR) at the Earth's surface is the largest component of the surface energy budget, being nearly double the downward shortwave radiation (DSR) (Kiehl and Trenberth, 1997). DLR has shown a remarkable increase during the process of global warming (Stephens et al., 2012). This is closely related to the fact that both a warming and moistening of the atmosphere (especially at the lower atmosphere associated with the water vapor feedback) positively contribute to this change. Understanding of complex spatiotemporal variation of DLR and its implication is necessary for improving weather prediction, climate simulation as well as water cycling modeling. Unfortunately, errors in DLR are considered substantially larger than errors in any of the other components of surface energy balance, which is most likely related to the lack of DLR measurements with high quality (Stephens et al., 2012).

The 2-sigma uncertainty of DLR measurement by using a well-calibrated and maintained pyrgeometer is estimated to be 2.5% or 4 $W \cdot m^{-2}$ (Stoffel, 2005). However, global-wide surface observations are very limited, especially in those remote regions. On the other hand, it has been known for almost one century that clear-sky DLR is determined by the bulk emissivity and effective temperature of the overlying atmosphere (Ångström, 1918). Since these two quantities are not easily observed for a vertical column of the atmosphere, clear-sky DLR is widely parameterized as a function of surface air temperature and water vapor density, assuming that the clear sky radiates toward the surface like a grey body at screen-level temperature. Dozens of parameterization formulas of DLR have been developed in which clear-sky effective emissivity (ε_c) is a function of the screen-level temperature (T) and water vapor pressure (e), or simply in the localized coefficients with given functions. Two formulas, i.e., an exponential function (Idso, 1981) and a power law function (Brunt, 1932; Swinbank, 1963), have been widely used to depict the relationship of ε_c to T and e. The coefficients of these functions are derived by a regression analysis of collocated measurements of T, e and DLR. Most of these proposed parameterizations are empirical in nature and only specific for definite atmospheric condition. An exception is that Brutsaert (1975) developed a model based on the analytic solution of the Schwarzchild's equation for a

standard atmospheric lapse rates of T and e. Prata (1996) found that the precipitable water content (w) was much better to represent the effective emissivity of the atmosphere than e, which was loosely based on radiative transfer simulations. Dilley and O'Brien (1998) adopted this scheme but tuned empirically their parameterization using an accurate radiative transfer model. Since DLR is to some extent impacted by water vapor and temperature profile (especially in case of existence of an inversion layer) and diurnal variation of T, a new model with two more coefficients considering these effects was developed (Dupont et al., 2008a).

In the presence of clouds, total effective emissivity of the sky is remarkably modulated by clouds. The existing clear-sky parameterization should be modified according to the cloud fraction (CF) and other cloud parameters such as cloud base height (CBH). CF is generally used to represent a fairly simple cloud modification under cloudy conditions. Dozens of equations with cloudiness correction have been developed and evaluated by DLR measurements across the world (Crawford and Duchon, 1999; Niemela et al., 2001). CF can be obtained by trained human observers (Iziomon et al., 2003) or derived from DSR (Crawford and Duchon, 1999) and DLR measurements (Durr and Philipona, 2004). High temporal resolution of DSR or DLR measurements (for example, 1-minute) can also provide cloud type information (Duchon and O'Malley, 1999), and thereby allow to consider potential effects of cloud types on DLR (Orsini et al., 2002).

With an average altitude exceeding 4 km above the sea level (ASL), the Tibetan Plateau (TP) exerts a huge influence on regional and global climate through mechanical and thermal forcing because of its highest and most extensive highland in the world (Duan and Wu, 2006). TP, compared to other high altitude regions and the poles, has been relatively more sensitive to climate change. The most rapid warming rate over the TP occurred in the latter half of the 20th century was likely associated with relatively large increase in DLR. Duan and Wu (2006) indicated that increase in low level nocturnal cloud amount and thereby DLR could partly explain the increase in the minimum temperature, despite decrease in total cloud amount during the same period. By using observed sensitivity of DLR to change in specific humidity for the Alps,

Rangwala et al. (2009) suggested that increase in water vapor appeared to be partly responsible for the large warming over the TP. Since the coefficients of certain empirical parameterizations and their performances showed spatiotemporal variations, establishment of localized DLR parameterizations over the TP is of highly significance. Further studies on DLR, including its spatiotemporal variability, its parameterization as well as its sensitivity to changes in atmospheric variables, would be expected to improve our understanding of climate change over the TP (Wang and Dickinson, 2013).

DLR measurements from high quality radiometer with high temporal resolution over the TP are quite scarce. To the best of our knowledge, there are very few publications on DLR and its parameterization over the TP. Wang and Liang (2009) evaluated clear-sky DLR parameterizations of Brunt (1932) and Brutsaert (1975) at 36 globally distributed sites, in which DLR data at two TP stations were used. Yang et al. (2012) used hourly DLR data at 6 stations to study major characteristics of DLR and to assess the all-sky parameterization of Crawford and Duchon (1999). Zhu et al. (2017) evaluated 13 clear-sky and 10 all-sky DLR models based on hourly DLR measurements at 5 automatic meteorological stations. The Kipp & Zonen CNR1 is composed of CM3 pyranometer and CG3 pyrgeometer that are used to measure DLR and DSR, respectively. The CG3 is the second class radiometer according to the International Organization for Standardization (ISO) classification. The root mean square of hourly DLR is less than 5 Wm^{-2} after field recalibration and window heating correction (Michel et al., 2008). Note that human observations of cloud every 3-6 hours or hourly DLR and DSR data are respectively used to determine clear sky and cloud cover in these previous studies.

In order to further our understanding of DLR and DSR over the TP, measurements of 1-minute DSR and DLR at 3 stations over the TP using state-of-the-art instruments have been performed in summer months since 2011. These data provide us opportunity to evaluate clear-sky DLR models and quantitatively assess cloud impacts on DLR. This study makes progress in the following aspects as compared to previous studies: 1) clear-sky discrimination and CF estimation are based on 1-minute DSR and DLR measurements that are objective in nature; 2) misclassification of cloudiness into cloud-

free skies would be minimized by adopting strict cloud-screening procedures based on 1-minute DSR, DLR and Lidar measurements; 3) potential effects of CBH on DLR are also investigated. Localized parameterizations of clear-sky and all-sky DLRs are finally achieved, which would be expected to improve DLR estimations over the TP.

2. Site, Instrument and Data

Measurements of DLR and DSR are conducted 1~4 months over the TP at three stations (Table 1), including Nagqu (NQ, 92.04°E, 31.29°N, 4507 m ASL), Nyingchi (NC, 94.2°E, 29.4°N, 2290 m ASL) and Ali (AL, 80°E, 32.5°N, 4287 m ASL). DLR and DSR were respectively measured by CG4 and CM21 radiometers (Kipp & Zonen, Delft, Netherlands). The sampling frequency is 1 Hz and the averages of the samples over 1-minute intervals are logged on a Campbell Scientific CR23X datalogger. Simultaneous 1-minute averages of T and e are taken from the automatic meteorological stations. With the aid of its specific material and unique construction, CG4 is designed for the DLR measurement with high reliability and accuracy. Window heating due to absorption of solar radiation in the window material, the major error source of DLR measurement, is strongly suppressed by its unique construction conducting away the absorbed heat very effectively. CM21 is a high performance research grade pyranometer. Introduction of individually optimized temperature compensation for CM21 makes it having much a smaller thermal offset than CM3. The installation of the CG4 and CM21 on the Kipp & Zonen CV2 ventilation unit prevents dew deposition on the window of the CG4 and the quartz dome of the CM21. The radiometers are calibrated before and after field measurements to the standards held by the China National Centre for Meteorological Metrology.

A Micropulse Lidar (MPL-4B, Sigma Space Corporation, United States) was installed site-by-site with radiometers. The Nd:YLF laser of the MPL produces an output power of 12 μJ at 532 nm. The repletion rate is 2500 Hz. The vertical resolution of the MPL data is 30 m and the integration time of the measurements is 30s. The MPL backscattering profiles are used to identify the cloud boundaries and derive the CBHs (He et al., 2013). The dataset contains about 700 hours of coincident DLR, DSR, Lidar

and meteorological measurements.

3. Methods

3.1 Clear-sky discrimination

Clear skies should be discriminated from cloudy conditions before performing DLR parametrization, which is achieved by the synthetical analysis of DSR, DLR, and CBH from MPL.

Following the method initiated by Crawford and Duchon (1999), we calculate two quantities reflecting DSR magnitude and variability based on 1-minute observed DSR (DSR_{obs}) and calculated clear-sky DSR (DSR_{cal}) values. DSR_{cal} is calculated by the model C of Iqbal (1983), in which direct and diffuse DSR are parametrized separately. Direct DSR (DSR_{dir}) is calculated as follows.

$$DSR_{dir} = S_0 \tau_r \tau_W \tau_o \tau_a \tau_g \quad (1)$$

where τ_r, τ_w, τ_o, τ_a and τ_g are transmittances due to Rayleigh scattering, water vapor absorption, ozone absorption, aerosol extinction and absorption by uniformly mixed gases O_2 and CO_2, respectively. Diffuse radiation is estimated as the sum of Rayleigh and aerosol scattering as well as multiple reflectance. Total ozone column (DU) is provided by Brewer spectrophotometer. *w* values (cm) are from Vaisala-92 radiosonde profiles in AL and Global Position System measurements in NC and NQ, respectively. They are used to create linear regression relationship to collocated ground level *e* (hPa) measurements, which is then used to estimate *w* from 1-minute measurements of *e*. Ångström wavelength exponent and Ångström turbidity are from CIE-318 sunphotometer observations in NC and AL, while in NQ we adopt the same value as that in AL. Mean single scattering albedo retrieved from CIE-318 observation in Lhasa (91.13, 29.67, 3663m) is 0.90 (Che et al., 2019), which is used in three stations. Surface Albedo is 0.25 and 0.22 in Al and NQ according to in situ measurements (Liang et al., 2012). In NC, it is 0.183 (Zhao et al., 2011).

DSR_{cal} values are first scaled to a constant value of 1400 $W \cdot m^{-2}$ for each minute of each day. We adopt this value according to Duchon and O'Malley (1998) and Long and Ackerman (2000), which only favors for a clear presentation of the normalized and

observed DSR values in the same figure. Afterwards, DSR_{obs} values are scaled by multiplying the same set of scale factors. Finally, the mean and standard deviation of the scaled DSR in a 21-minute moving window (±10 minute centered on the time of interest) are used for cloud screening. Selection of the width of 21-minute is empirical but a consequence of having a reasonable time span for estimating the mean and variance (Duchon and O'Malley, 1999). Clear-sky DSR should satisfy three requirements: 1) ratio of DSR_{obs} to DSR_{cal} is within 0.95 to 1.05; 2) difference between scaled DSR_{obs} and DSR_{cal} is less than 20 $W \cdot m^{-2}$; and 3) standard deviation (δ) of scaled DSR_{obs} in a 21-minute moving window is less than 20 $W \cdot m^{-2}$.

Temporal variability of DLR is also used for cloud screening according to Marty and Philipona (2000) and Sutter et al. (2004). Here, δ of scaled DLR (scaled to 500 $W \cdot m^{-2}$) in a 21-minute moving window is used for this purpose. Cloud-free sample is determined if δ is less than 5 $W \cdot m^{-2}$.

Since both DSR and DLR experience difficulties in detecting clouds in the portion of the sky far away from the sun (Duchon and Malley, 1999) or high-altitude cirrus clouds (Dupont et al., 2008b), coincident MPL backscatter measurements are used to strictly select clear-sky samples. There should be a cloud element somewhere in the sky when MPL identifies cloud, it is thus required that no clouds are detected by MPL in a 21-minute moving window, otherwise it is defined as cloudy.

Given the fact that these methods are complementary to each other to some extent (Orsini et al., 2002), we use the following strategy to guarantee a proper selection of clear-sky samples. If DSR, DLR and MPL measurements at the time of interest synchronously satisfy these specified clear-sky conditions, the sample is thought to be taken under unambiguously cloud-free condition; on the contrary, the measurement are made under unambiguously cloudy condition if any method suggests cloudy. Our following clear-sky and cloudy DLR parameterizations are respectively based on measurements under unambiguously cloud-free (8195 minutes) and cloudy conditions (69318 minutes).

Fig. 1 shows an example of clear sky discrimination results based on our method. DSR_{obs} presents a smooth temporal variation from sunrise to about 14:00 (LST), being

consistent with DSR_{clr}. Similarly, DLR also varies very smoothly during the same period when 21-minute standard deviations of DLR are < 5 $W \cdot m^{-2}$. Both facts suggest sunny and cloudless skies. This inference is supported by MPL that suggests no cloud detected overhead. Contrarily, an abruptly changes of 1-minute DSR_{obs} and DLR are evident during 14:00~17:00 LST and we can see DSR_{obs} occasionally exceeds the expected DSR_{clr}, indicating frequent occurrence of fair weather cumuli clouds. MPL detect a persistent thin cloud layer at 4 km above ground, which agrees with DSR and DLR measurements very well.

3.2 Cloud fraction estimation

Given synoptic cloud observations are very limited and temporally sparse, various parameterizations using DSR or DLR data have been developed to estimate CF (e.g., Deardorff, 1978; Marty and Philipona, 2000; Durr and Philipona, 2004; Long et al., 2006; Long and Turner, 2008). Because of good agreement between clear-sky DSR_{obs} and DSR_{cal} calculated by the Iqbal C calculations (Iqbal, 1983; Gubler et al., 2012), with mean bias of 1.7 $W \cdot m^{-2}$ and root mean square error (RMSE) of 10.7 $W \cdot m^{-2}$ (not shown), we use Deardorff (1978)'s method to calculate CF from DSR_{obs} and DSR_{cal}. The method is based on a fairly simple cloud modification to DSR as follows.

$$\mathrm{CF} = 1 - \frac{\mathrm{DSR}_{obs}}{\mathrm{DSR}_{cal}} \qquad (2)$$

CF (no unit) has values ranging from 0 to 1. To avoid the error caused by abrupt DSR variation, 21-minute mean DSR value rather than its instantaneous measurements are used here.

4 Results

4.1 Clear-sky DLR parameterization evaluation and localization

Eleven clear-sky DLR (DLR_{clr}) parameterizations (Table 2) are evaluated based on 1-minute DLR measurements under unambiguously cloud-free conditions. To compare the performance of these 11 models, RMSE and the coefficient of determination (R^2) are shown by a Taylor diagram in Fig. 2(a). Relatively smaller

RMSE (generally < 15 $W \cdot m^{-2}$) and larger R^2 (>0.95) are derived for the Brutsaert (1975); Konzelmann (1994), Dilley and O'Brien (1998) and Prata (1996) models. This is likely because these parameterizations were developed in cool and dry areas, for example, in England (Brutsaert, 1975); in Greenland (Konzelmann, 1994) and dry desert region in Australia (Prata, 1996). The climate in those areas is likely similar to that over the TP to some extent, so those parameterizations are expected to perform well. The higher RMSE (>37 $W \cdot m^{-2}$) and the lower R^2 (~0.7) are derived for Swinbank (1963) and Idso and Jackson (1969) models. This can be partly explained by the fact that only T is used in these two methods. Previous studies suggests substantial uncertainty (RMSE >37.5 $W \cdot m^{-2}$ and R^2 <0.75) if water vapor effect on DLR_{clr} is not accounted for (Duarte et al., 2006). Since w is very low over the TP and thereby DLR is highly sensitive to variation of w in that case, much more attention should be paid to water vapor effect on the parameterization of DLR_{clr}.

The coefficients in eleven parameterizations (Table 2) were originally calibrated and determined in different geographical locations; therefore, they may not be the optimal values for the TP. Thus we take use of 1-minute clear-sky DLR samples to locally calibrate the parameters of these parametrizations. We use 10-fold cross-validation method to determine the parameters. This is a widely used method to estimate the skill of a regression model on unseen data. It is expected to result in a less biased or less optimistic estimate of the model skill than other methods, such as a simple train/test split (James et al., 2013). All the data was randomly dividing into 10 groups of approximately equal size, the coefficients are computed by using 9 groups as training set, and the remaining 1 group is used as validation. This procedure is repeated 10 times to get the representational value of coefficients (with the lowest test error).

The coefficient values derived from the non-linear least-squares fitting of the DLR_{clr} parameterizations (Table 2) over the TP are presented in Table 3. For each fitted parameterization, we calculated RMSE and R^2 and the results are shown in Fig. 2b. When using the parameterizations with the locally fitted parameters, the accuracy of the parameterization relative to the published values is obviously improved. Most RMSEs are < 10 $W \cdot m^{-2}$ except the parameterization proposed by Swinbank (1963) and

Idso and Jackson (1969) that still produce the worst results (with R^2 of 0.71 and RMSE of 15 W·m^{-2}) even after the parameters are locally calibrated.

The Dilley and O'Brien (1998)'s parameterization, which is initially developed by considering the adaptation of climatological diversities, is expected to be able to fit the measurements in tropical, mid-latitude and Polar Regions. This expectation is verified by its wide deployment in DLR_{clr} estimations in different climate regimes and altitude levels, for example, in the tropical lowland (eastern Pará state, Brazil) and the mild mountain area (Boulder, the United States) (Marthews et al., 2012; Li et al., 2017). The present study confirms that Dilley and O'Brien (1998) is the best clear-sky parameterization over the TP. The locally calibrated equation is as follows.

$$DLR_{clr} = -2.53 + 158.10 \times \left(\frac{T}{273.16}\right)^6 + 106.40 \times \left(\frac{46.50 \times \frac{e}{T}}{2.50}\right)^{\frac{1}{2}} \quad (3)$$

Where T and e represent air temperature (K) and water vapor pressure (hPa), respectively (T and e have the same meaning and unit in following equations if not specified). The RMSE and R^2 of Eq.(3) are ~3.8 W·m^{-2} and > 0.98 respectively, which are substantially lower than those in previous studies over the TP, for example, the RMSE was 9.5 W·m^{-2} (Zhu et al., 2017). The Dilley and O'Brien (1998)'s parameterization was suggested to be the most reliable estimates of DLR_{clr} over the TP (Zhu et al., 2017). Note that the parameters here differ quite a lot from their values (Zhu et al., 2017), as shown in Eq. (4).

$$DLR_{clr} = 30.00 + 157.00 \times \left(\frac{T}{273.16}\right)^6 + 97.93 \times \left(\frac{46.50 \times \frac{e}{T}}{2.50}\right)^{\frac{1}{2}} \quad (4)$$

Fig.3 compares instantaneous clear-sky DLR data from measurements against calculations by Eq. (3) of this study and by Eq. (4) from Zhu et al. (2017). The former performs very well as shown by an overwhelmingly large number of data points falling along or overlapping the 1:1 line. By contrast, the latter overestimates DLR by 25 W·m^{-2} (10%). This difference is not very likely due to different DLR measurements used to produce Eq. (3) and (4) giving the following considerations. First, this systematic overestimation is much larger than the expected uncertainty of DLR measurements (2.5% or 4 W·m^{-2}) (Stoffel, 2005). More important, comparison of cloudy DLR parameterizations between this study and Zhu et al. (2017) showed good agreement

(not shown). Note that only 1-hour CG3 DLR observations are used for clear sky discrimination in Zhu et al. (2017). This method was shown to be very likely contaminated by the thin high cloud (Sutter et al., 2004). This certainly would produce an overestimation of clear sky DLR parameterization since larger DLRs are associated with potential residual clouds relative to real clear sky DLRs.

4.2 Parameterization of cloudy-sky DLR

Parameterizations of cloudy-sky DLR (DLR_{cld}) are based on estimated DLR_{clr} coupled with the effect of cloudiness or cloud emissivity, which depends primarily on CF as well as other cloud parameters, like CBH and cloud type (Arking, 1990; Viúdez-Mora et al., 2015). Four parameterizations (Table 4), which modifies the bulk emissivity depending on CF, are assessed and locally calibrated in this section.

DLR_{clr} is estimated according to Eq. (3). The fitted values of the coefficients (using 10-Fold Cross-Validation) of the four cloudy parameterizations are presented in Table 5. RMSE and R^2 of original and locally fitted parameterizations over the TP are presented in Fig. 4.

Relative to clear-sky conditions, cloudy parameterizations using the given parameters have higher error RMSE (generally exceeding 35 $W \cdot m^{-2}$) except that developed by Jacobs (1978) (RMSE of 18 $W \cdot m^{-2}$). R^2 was generally smaller than 0.9. RMSE values decrease significantly in Maykut and Church (1973) and Sugita and Brutsaert (1993) as locally calibrated parameters are used. Relative smaller and almost no RMSE improvements are found for the methods developed by Konzelmann (1994) and Jacobs (1978).

Eq. (5) shows the best cloudy-sky parameterization over the TP by combining the clear-sky parameterization of Dilley and O'Brien (1998) with the cloud modulation correction scheme of Jacobs (1978).

$$\mathrm{DLR}_{cld} = (1 + 0.23 \times \mathrm{CF}) \times \left(59.38 + 113.70 \times \left(\frac{T}{273.16}\right)^{6} + 96.96 \times \left(\frac{46.50 \times \frac{e}{T}}{2.50}\right)^{\frac{1}{2}}\right) \quad (5)$$

RMSE and R^2 are ~18 $W \cdot m^{-2}$ and ~0.89 respectively. RMSE here is close to 15 $W \cdot m^{-2}$ obtained in different altitude areas in Swiss (Gubler et al., 2012) and slightly lower than 23 $W \cdot m^{-2}$ obtained in mountain area in Germany (Iziomon et al., 2003). Comparing to

previous studies over the TP (RMSE of 22 W m^{-2} in Zhu et al., 2017), our cloudy model produces better results.

4.3 Effect of CBH on DLR under Overcast Conditions

Since clouds behave approximately as a blackbody, the most relevant cloud parameter (besides CF) to DLR under overcast skies (DLR_{ovc}) is the temperature of its lower boundary (CBH). Radiative transfer model simulation has suggested that CBH under overcast conditions is an important modulator for DLR. The cloud radiation effect (CRE), the difference between DLR_{obs} and DLR_{clr}, decreases with increasing CBH at a rate of 4~12 W·m^{-2} that depends on climate profiles (Viúdez-Mora et al., 2015). This indicates that cloudy DLR parameterization would be improved if CBH is considered.

The statistical relationship between CRE and CBH under overcast conditions over the TP is presented in Fig. 5. The peak and median values of CRE decrease with the increase of CBH from the box plot in Fig.5. CRE variation increases from 25 to 50 W·m^{-2} as CBH increases because water vapor influence and its variation goes up. Compared to Viúdez-Mora (2015) results derived at Girona, Spain, a mid-latitude site with low altitude, CRE over the TP is generally lower by 5~10 W·m^{-2}. This is likely because clouds over the TP with the same CBH as that at Girona have relatively lower temperature, thereby producing lower radiative effect on DLR. It is interesting that the decreasing tendency of CRE with CBH is apparent. CRE is about 70 W·m^{-2} for clouds < 1 km and decreases to ~40 W·m^{-2} for clouds at 3~4 km in TP. The decreasing rate of CRE with CBH is estimated to be -9.8 W·m^{-2}·km^{-1} over the TP that agrees with model simulations (Viúdez-Mora et al., 2015).

To consider CBH effect under overcast conditions, we introduced a modified parameterization according to Viúdez-Mora et al. (2015):

$$\mathrm{DLR}_{ovc} = 1.23 \times \mathrm{DLR}_{clr} \times (1.01 - 0.06 \times \mathrm{CBH}) \quad (6)$$

Where CBH has unit of km. The bias and RMSE of Eq. (6) between measurements and calculations is 1.3 W·m^{-2} and 16.5 W·m^{-2}, respectively, which are significantly

lower than that of Eq. (5) (10.3 $W \cdot m^{-2}$ and 21.4 $W \cdot m^{-2}$) in overcast conditions. The result indicates a remarkable improvement in the estimation of DLR under overcast conditions by introducing CBH to the DLR parameterization.

5 Discussion and conclusions

The parameterization of clear-sky DLR requires a well-defined distinction between clear-sky and cloudy-sky situations that commonly depends on human cloud observations 4~6 times each day. Human observation is subjective in nature and its low temporal resolution cannot resolve dramatic high-resolution variation of clouds. Furthermore, synoptic human cloud observations show the tendency to stronger weight to the horizon that DLR is not highly sensitive (Marty and Philipona, 2004). Clear sky discrimination based on hourly DSR or DLR measurements also tends to be very suspect of residual clouds due to their low temporal resolution. Parameterization of clear-sky DLR based on these two methods is hence very likely biased as a consequence of selection of cloud contaminated clear-sky measurements. This would result in biased estimation of cloud DLR effect since it is the difference between clear-sky and measured all-sky DLRs (Dupont et al., 2008b).

Using 1-minute DSR and DLR at 3 stations over the TP, DLR parameterizations are evaluated and localized parameterizations have been developed based on a comprehensive cloud-screening method. Potential CBH effect on overcast DLR is experimentally determined. Major conclusions are as follows.

Among 11 clear-sky DLR parameterizations tested in this study, two methods using only atmospheric temperature largely deviate from other parameterizations. The best method suitable for TP is the parameterization developed by Dilley and O'Brien (1998). DLR estimation can be improved by localization of these parameterizations. Locally calibrated parameterization can produce clear sky DLR with RMSE of 3.8 $W \cdot m^{-2}$.

Overcast DLR is highly sensitive to CBH. The parameterization can be substantially improved by consideration of CBH effect. The bias between empirically parameterized calculations and measurements decreases from 10.3 to 1.3 $W \cdot m^{-2}$.

The focus of this study is on daytime DLR parameterization over the TP since DSR is used in the cloud-screening method. Given a significant role of DLR played in the surface energy budget during nighttime, it is highly desirable to perform further study on the nighttime DLR parametrization. These results are based on summer DLR measurements, so the conclusions here need to be further tested in other seasons, especially in winter when an increasing tendency of DLR has been observed (Rangwala et al., 2009). Further investigations on these issues are expected to shed new light on how and why DLR has changed over the TP.

Acknowledgements: This work was supported by the Strategic Priority Research Program of Chinese Academy of Sciences (XDA17010101), the National Key R&D Program of China (2017YFA0603504), the National Natural Science Foundation of China (91537213 and91637107), the Special Fund for Meteorological Research in the Public Interest (GYHY201106023), and the Science and Technological Innovation Team Project of Chinese Academy of Meteorological Science (2013Z005) respectively support the observations at AL, NQ and NC. We greatly appreciate Dr. Q. He for providing the MPL Lidar measurement images and derived CBH data.

References

Ångström, A.: A study of the radiation of the atmosphere, Smithsonian Miscellaneous Collection, 65, 1–159, 1915.

Arking, A.: The radiative effects of clouds and their impact on climate, Bull. Am. Meteorol. Soc., 72, 795-813, 10.1175/1520-0477(1991)072<0795:Treoca>2.0.Co;2, 1991.

Brunt, D.: Notes on radiation in the atmosphere, Q. J. Roy. Meteorol. Soc., 58, 389–420, 1932.

Brutsaert, W.: On a derivable formula for long-wave radiation from clear skies, Water Resource Res., 11, 742–744, 1975.

Carmona, F., Rivas, R., and Caselles, V.: Estimation of daytime downward longwave radiation under clear and cloudy skies conditions over a sub-humid region, Theor. Appl. Climatol., 115, 281-295, 10.1007/s00704-013-0891-3, 2014.

Che, H. Z., Zhao, H. J., Wu, Y. F., Xia, X. G., Zhu, J., Wang, H., Wang, Y. Q., Sun, J. Y., Yu, J., Zhang, X. Y., and Shi, G. Y.: Analyses of aerosol optical properties and direct radiative forcing over urban and industrial regions in Northeast China, Meteorol. Atmos. Phys., 127, 345-354, 10.1007/s00703-015-0367-3, 2015.

Che, H., Xia, X., Zhao, H., Dubovik, O., Holben, B. N., Goloub, P., Cuevas-Agulló, E., Estelles, V., Wang, Y., Zhu, J., Qi, B., Gong, W., Yang, H., Zhang, R., Yang, L., Chen, J., Wang, H., Zheng, Y., Gui, K., Zhang, X., and Zhang, X.: Spatial distribution of aerosol microphysical and optical properties and direct radiative effect from the China Aerosol Remote Sensing Network, Atmos. Chem. Phys. Discuss., https://doi.org/10.5194/acp-2019-405, 2019.

Crawford, T. M., and Duchon, C. E.: An improved parameterization for estimating effective atmospheric emissivity for use in calculating daytime downwelling longwave radiation, J. Appl. Meteorol., 38, 474–480, 1998.

Deardorff, J. W.: Efficient prediction of ground surface temperature and moisture, with an inclusion of a layer of vegetation. J. Geophys. Res., 83, 1889–1903, 1978.

Dilley, A. C., and O'Brien, D. M.: Estimating downward clear sky long-wave irradiance at the surface from screen temperature and precipitable water, Q. J. Roy. Meteorol. Soc., 124a, 1391–1401, 1997.

Dozier, J., and Frew, J.: Rapid calculation of terrain parameters for radiation modeling from digital elevation data, IEEE T. Geosci. Remote, 28, 963–969, 1990.

448 Dominik, M., R. Philipona, C. Ruckstuhl, R. Vogt and L. Vuileumier, Performance and
449 uncertainty of CNR1 net radiometers during a one-year field comparison, J of
450 Atmos., and Ocean. Tech., 25(3), 442-451, 2008.
451 Duan, A., and Wu, G.: Change of cloud amount and the climate warming on the Tibetan
452 Plateau, Geophys. Res. Lett., 33, 10.1029/2006gl027946, 2006.
453 Duarte, H. F., Dias, N. L., and Maggiotto, S. R.: Assessing daytime downward
454 longwave radiation estimates for clear and cloudy skies in Southern Brazil, Agr.
455 Forest. Meteorol., 139, 171-181, 10.1016/j.agrformet.2006.06.008, 2006.
456 Duchon, C. E., and O'Malley, M. S.: Estimating cloud type from pyranometer
457 observations, J. Appl. Meteorol., 38, 132-141, 1999.
458 Dupont, J. C., Haeffelin, M., Drobinski, P., and Besnard, T.: Parametric model to
459 estimate clear-sky longwave irradiance at the surface on the basis of vertical
460 distribution of humidity and temperature, J. Geophys. Res., 113,
461 10.1029/2007jd009046, 2008.
462 Durr, B., and Philipona, R.: Automatic cloud amount detection by surface longwave
463 downward radiation measurements, J. Geophys. Res., 109, 9,
464 10.1029/2003jd004182, 2004.
465 Gubler, S., Gruber, S., and Purves, R. S.: Uncertainties of parameterized surface
466 downward clear-sky shortwave and all-sky longwave radiation, Atmos. Chem.
467 Phys., 12, 5077-5098, 10.5194/acp-12-5077-2012, 2012.
468 He, Q. S., Li, C. C., Ma, J. Z., Wang, H. Q., Shi, G. M., Liang, Z. R., Luan, Q., Geng,
469 F. H., and Zhou, X. W.: The properties and formation of cirrus clouds over the
470 Tibetan Plateau based on summertime lidar measurements, J. Atmos. Sci., 70, 901-
471 915, 10.1175/jas-d-12-0171.1, 2013.
472 Idso, S. B.: A set of equations for full spectrum and 8 to 14 μm and 10.5 to 12.5 μm
473 thermal radiation from cloudless skies, Water Resource Res., 17, 295–304, 1981.
474 Iqbal, M.: An Introduction to Solar Radiation, Academic Press, Toronto, Canada, 1983.
475 Iziomon, M. G., Mayer, H., and Matzarakis, A.: Downward atmospheric longwave
476 irradiance under clear and cloudy skies: measurement and parameterization, J.
477 Atmos. Solar-Terr. Phys., 65, 1107–1116, 2003.
478 Jacobs, J.D.: Radiation climate of Broughton Island, in: Energy Budget Studies in
479 Relation to Fast-ice Breakup Processes in Davis Strait, edited by Barry, R. G. and
480 Jacobs, J. D., Inst. of Arctic and Alp. Res. Occas. Paper No. 26. University of
481 Colorado, Boulder, pp. 105–120, 1978.

James, G., Witten, D., Hastie, T., and Tibshirani, R.: An Introduction to Statistical Learning: with Applications in R, Springer-Verlag New York, USA, 2013.

Kiehl, J. T., and Trenberth, K. E.: Earth's annual global mean energy budget. Bull. Am. Meteorol. Soc., 78, 197-208, 1997.

Konzelmann, T., van de Wal, R. S. W., Greuell, W., Bintanja, R., Henneken, E. A. C., and Abe-Ouchi, A.: Parameterization of global and longwave incoming radiation for the Greenland Ice Sheet, Global Planet. Change, 9, 143–164, 1994.

Kruk, N. S., Vendrame, I. F., da Rocha, H. R., Chou, S. C., and Cabral, O.: Downward longwave radiation estimates for clear and all-sky conditions in the Sertozinho region of So Paulo, Brazil, Theor. Appl. Climatol., 99, 115-123, 2010.

Li, M. Y., Jiang, Y. J., and Coimbra, C. F. M.: On the determination of atmospheric longwave irradiance under all-sky conditions, Sol. Energy., 144, 40-48, 10.1016/j.solener.2017.01.006, 2017.

Liang, H., Zhang, R. H., Liu, J. M., Sun, Z. A., and Cheng, X. H.: Estimation of hourly solar radiation at the surface under cloudless conditions on the Tibetan Plateau using a simple radiation model, Adv. Atmos. Sci., 29, 675-689, 10.1007/s00376-012-1157-1, 2012.

Long, C. N., Ackerman, T. P., Gaustad, K. L., and Cole, J. N. S.: Estimation of fractional sky cover from broadband shortwave radiometer measurements, J. Geophys. Res., 111, 11, 10.1029/2005jd006475, 2006.

Long, C. N., and Turner, D. D.: A method for continuous estimation of clear-sky downwelling longwave radiative flux developed using ARM surface measurements, J. Geophys. Res., 113, 16, 10.1029/2008jd009936, 2008.

Marthews, T. R., Malhi, Y., and Iwata, H.: Calculating downward longwave radiation under clear and cloudy conditions over a tropical lowland forest site: an evaluation of model schemes for hourly data, Theor. Appl. Climatol., 107, 461-477, 10.1007/s00704-011-0486-9, 2012.

Marty, C., and Philipona, R.: The Clear-Sky Index to separate clear-sky from cloudy-sky situations in climate research, Geophys. Res. Lett., 27, 2649-2652, 10.1029/2000gl011743, 2000.

Maykut, G. A., and Church P. E.: Radiation climate of Barrow, Alaska, 1962–1966, J. Appl. Meteorol., 12, 620–628, 1973.

Niemelä, S., Räisänen, P., and Savijärvi, H.: Comparison of surface radiative flux parameterizations: Part I: Longwave radiation, Atmos. Res., 58, 1–18, 2001a.

516 Orsini, A., Tomasi, C., Calzolari, F., Nardino, M., Cacciari, A., and Georgiadis, T.:
517 Cloud cover classification through simultaneous ground-based measurements of
518 solar and infrared radiation, Atmos. Res., 61, 251-275, 10.1016/s0169-
519 8095(02)00003-0, 2002.
520 Prata, A. J.: A new long-wave formula for estimating downward clear-sky radiation at
521 the surface, Q. J. Roy. Meteorol. Soc., 122, 1127–1151, 1996.
522 Rangwala, I., Miller, J. R., and Xu, M.: Warming in the Tibetan plateau: possible
523 influences of the changes in surface water vapor. Geophys. Res. Lett., 36, 295-311,
524 2009.
525 Satterlund, D. R.: An improved equation for estimating longwave radiation from the
526 atmosphere, Water Resource Res., 15, 1649–1650, 1979.
527 Stephens, G. L., Wild, M., Stackhouse, P. W., Jr., L'Ecuyer, T., Kato, S., and Henderson,
528 D. S.: The global character of the flux of downward longwave radiation, J.
529 Climate., 25, 2329-2340, 10.1175/jcli-d-11-00262.1, 2012.
530 Stoffel, T.: Solar infrared radiation station (SIRS) handbook, Tech. Rep., ARM TR-025,
531 Atmos. Rad. Mea. Program, U.S. Dep. of Energy, Washington, D.C, 2005.
532 Sugita, M., and Brutsaert, W.: Cloud effect in the estimation of instantaneous downward
533 longwave radiation, Water Resource Res., 29, 599-605, 10.1029/92wr02352, 1993.
534 Swinbank, W. C.: Long-wave radiation from clear skies, Q. J. Roy. Meteo. Soc., 89,
535 330–348, 1963.
536 Viúdez-Mora, A., Costa-Surós, M., Calbó, J., and González, J. A.: Modeling
537 atmospheric longwave radiation at the surface during overcast skies: The role of
538 cloud base height, J. Geophys. Res. Atmos., 120, 199–214, 10.1002/
539 2014JD022310, 2015.
540 Wang, K., and Liang, S.: Global atmospheric downward longwave radiation over land
541 surface under all-sky conditions from 1973 to 2008, J. Geophys. Res., 114,
542 10.1029/2009jd011800, 2009.
543 Wang, K., and Dickinson, R. E.: Global atmospheric downward longwave radiation at
544 the surface from ground-based observations, satellite retrievals, and re-analyses,
545 Reviews of Geophysics, 51, 150-185, 10.1002/rog.20009, 2013.
546 Yang, K., Ding, B., Qin, J., Tang, W., Lu, N., and Lin, C.: Can aerosol loading explain
547 the solar dimming over the Tibetan Plateau? Geophys. Res. Lett., 39,
548 10.1029/2012gl053733, 2012.
549 Zhao X., Peng B., Qin N., Wang W. (2011), Characteristics of Energy Transfer and

Micrometeorology in Surface Layer in Different Areas of Tibetan Plateau in Summer (in Chinese), Plateau and mountain Meteorology Research,31(1), 6-11, 2011.

Zhu, M. L., Yao, T. D., Yang, W., Xu, B. Q., and Wang, X. J.: Evaluation of parameterizations of incoming longwave radiation in the high-mountain region of the Tibetan Plateau, J. Appl. Meteorol. Climatol., 56, 833-848, 10.1175/jamc-d-16-0189.1, 2017.

Table 1: Description of stations and measurements (magnitude and variability) in the Tibetan Plateau

Site	Altitude (m ASL)	Period	T (℃)	e (hPa)	DLR ($W \cdot m^{-2}$)	Data Points
NQ	4507	2011.7.20-2011.8.26	9.4±8	7.4±5	242.75±40	52980
NC	2290	2014.6.7-2014.7.31	16.8±10	13.4±4	368.25±40	69609
AL	4279	2016.5.27-2016.9.22	7.8±4	4.8±4	253.11±50	86596

563 **Table 2.** 11 clear-sky DLR parameterizations and their specific conditions

Reference	Clear-Sky Parameterization	Conditions
Angstrom (1915)	$\mathrm{DLR}_{clr} = \{0.83 - 0.18 \times 10^{-0.067e})\}\sigma T^4$	Alt.: 1650~3500 *T*: 283.15~303.15 *e*: 4~1
Brunt (1932)	$\mathrm{DLR}_{clr} = (0.52 + 0.065\sqrt{e})\sigma T^4$	Alt.: 6~3500 *T*: 269.15~303.15 *e*: 2.5~16
Swinbank (1963)	$\mathrm{DLR}_{clr} = 5.31 \times 10^{-13} T^6$	Alt: 2 *T*: 281.15~302.15 *e*: 8~30
Idso and Jackson (1969)	$\mathrm{DLR}_{clr} = (1 - 0.261 \cdot \exp(-0.000777 \times (273 - \mathrm{T})^2))\sigma T^4$	Alt.: 3, 331 *T*: 228.15~318.15
Brutsaert (1975)	$\mathrm{DLR}_{clr} = 1.24\left(\frac{e}{T}\right)^{\frac{1}{7}}\sigma T^4$	Alt.: 6~3500 *T*: 269.15~313.15 *e*: 2.5~-16
Satterlund (1979)	$\mathrm{DLR}_{clr} = 1.08\left(1 - \exp\left(-e^{\frac{T}{2016}}\right)\right)\sigma T^4$	Alt.: 594 *T*: 236.15~309.15 *e*: 0~18hPa
Idso (1981)	$\mathrm{DLR}_{clr} = \left(0.7 + 5.95 \times 10^{-5} \times e \times \exp\left(\frac{1500}{T}\right)\right)\sigma T^4$	Alt.: 331 *T*: 258.15~278.15 *e*: 2~6
Konzelmann (1994)	$\mathrm{DLR}_{clr} = \left(0.23 + 0.443\left(\frac{e}{T}\right)^{\frac{1}{8}}\right)\sigma T^4$	Alt.: 340~3230 *T*: 257.15~279.15 *e*: 1.5~5.5
Prata (1996)	DLR_{clr}=(1-(1+46.5$\frac{e}{T}$) ×exp(-(1.2+3×46.5 $\frac{e}{T}$)$^{0.5}$)) σT^4	Not specified
Dilley and O'Brien (1998)	DLR_{clr}=59.38+113.7$\left(\frac{T}{273.16}\right)^6$ + 96.96$\sqrt{46.5\frac{e}{T}/2.5}$	Not specified
Iziomon (2001)	$\mathrm{DLR}_{clr} = \left(1 - 0.43\exp\left(-\frac{11.5e}{T}\right)\right)\sigma T^4$	Alt.: 1489 $\bar{T}$=277.55$\bar{e}$ =7.4

564 *Where Alt. is the altitude above sea level, and its unit is (m ASL), e is screen-level water vapor

565 pressure in hPa and *T* represents surface temperature in K

566

567

568

569 **Table 3.** Locally fitted clear-sky DLR parameterizations in TP

Reference	Locally fitted Clear-Sky Parameterization
Angstrom(1915)	$\mathrm{DLR}_{clr} = \{0.8 - 0.19 \times 10^{-0.068e})\}\sigma T^4$
Brunt(1932)	$\mathrm{DLR}_{clr} = (0.56 + 0.07\sqrt{e})\sigma T^4$
Swinbank(1963)	$\mathrm{DLR}_{clr} = 4.7 \times 10^{-13} T^6$
Idso & Jackson(1969)	$\mathrm{DLR}_{clr} = (1 - 0.36 \cdot \exp(-0.00065 \times (273 - T)^2))\sigma T^4$
Brutsaert(1975)	$\mathrm{DLR}_{clr} = 1.03\left(\frac{e}{T}\right)^{0.09}\sigma T^4$
Satterlun (1979)	$\mathrm{DLR}_{clr} = \left(1 - \exp\left(-e^{\frac{T}{2016}}\right)\right)\sigma T^4$
Idso(1981)	$\mathrm{DLR}_{clr} = \left(0.63 + 7.5 \times 10^{-5} \times e \times \exp\left(\frac{1500}{T}\right)\right)\sigma T^4$
Konzelmann(1994)	$\mathrm{DLR}_{clr} = \left(0.23 + 0.45\left(\frac{e}{T}\right)^{0.13}\right)\sigma T^4$
Prata(1996)	DLR_{clr}=(1-(1+46.5$\frac{e}{T}$) ×exp(-(1+3×46.5$\frac{e}{T}$)$^{0.5}$)) σT^4
Dilley and O'Brien(1998)	DLR_{clr}=-2.54+158.1$\left(\frac{T}{273.16}\right)^6 + 106.4\sqrt{46.5\frac{e}{T}/2.5}$
Iziomon(2001)	$\mathrm{DLR}_{clr} = \left(1 - 0.38\exp\left(-\frac{14.52e}{T}\right)\right)\sigma T^4$

570

571 **Table 4.** 4 Cloudy-sky DLR Parameterizations in the references

Reference	Cloudy-Sky Parameterization
Maykut and Church, 1973	$\mathrm{DLR}_{cld} = (0.7855 + 0.000312 \times \mathrm{CF}^{2.75})\sigma T^4$
Jacobs, 1978	$\mathrm{DLR}_{cld} = (1 + 0.26 \times \mathrm{CF})\mathrm{DLR}_{clr}$
Sugita and Brutsaert, 1993	$\mathrm{DLR}_{cld} = (1 + 0.0496 \times \mathrm{CF}^{2.45})\ \mathrm{DLR}_{clr}$
Konzelmann, 1994	$\mathrm{DLR}_{cld} = (1 - \mathrm{CF}^4)\mathrm{DLR}_{clr} + 0.954\mathrm{CF}^4\sigma T^4$

572
573
574

575

576 **Table 5.** Locally fitted cloudy-sky DLR parameterizations in TP

Reference	Locally fitted Cloudy-Sky Parameterization
Maykut and Church, 1973	$\mathrm{DLR}_{cld} = (0.85 + 0.01 \times \mathrm{CF}^3)\sigma T^4$
Jacobs, 1978	$\mathrm{DLR}_{cld} = (1 + 0.23 \times \mathrm{CF})\mathrm{DLR}_{clr}$
Sugita and Brutsaert,1993	$\mathrm{DLR}_{cld} = (1 + 0.2 \times \mathrm{CF}^{1.3})\ \mathrm{DLR}_{clr}$
Konzelmann, 1994	$\mathrm{DLR}_{cld} = (1 - \mathrm{CF}^{3.5})\mathrm{DLR}_{clr} + \mathrm{CF}^{3.5}\sigma T^4$

577

578

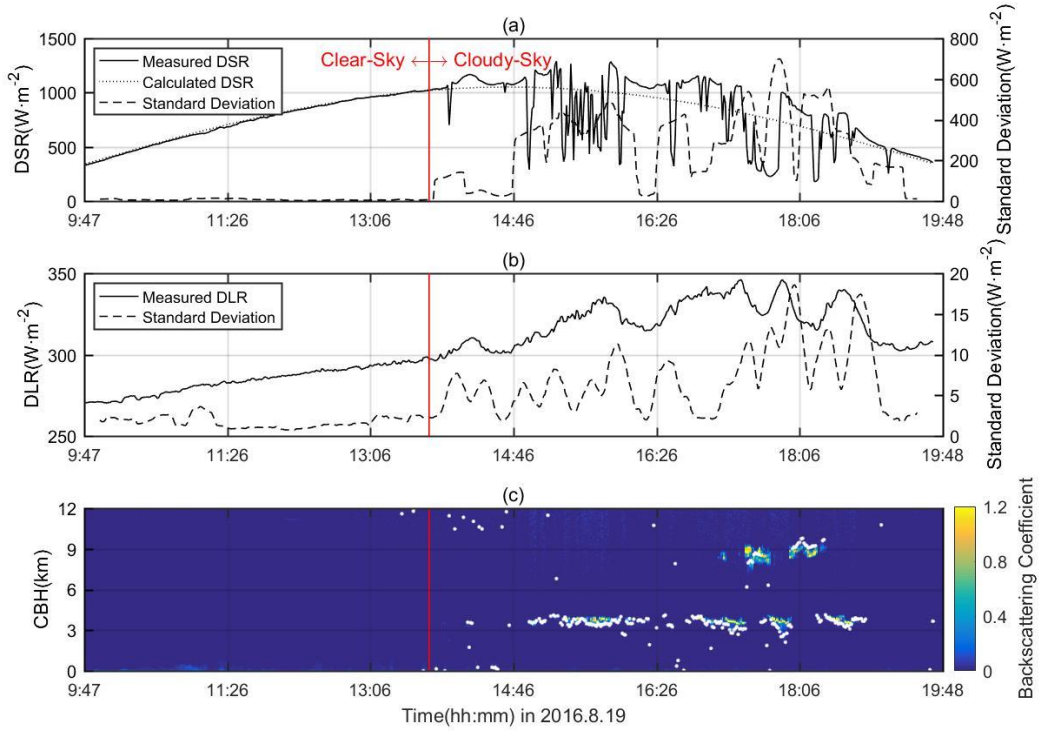

Fig. 1. Time series of data sample on 2016.8.19 transited from clear-sky to cloudy-sky: (a) measured (black line) and calculated (dotted black line) downward shortwave radiation and its 21-min standard deviation (grey line), (b) measured downward longwave radiation and 21-min standard deviation and (c) MPL backscattering coefficient and the cloud base height.

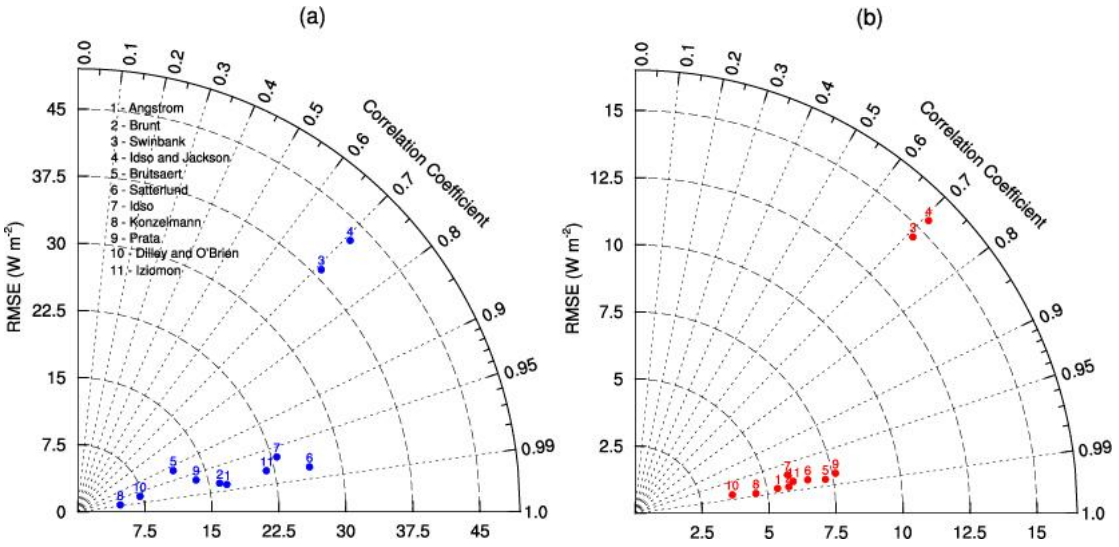

Fig. 2. RMSE and R^2 for the clear-sky DLR parameterizations using original (a) and locally calibrated (b) coefficients.

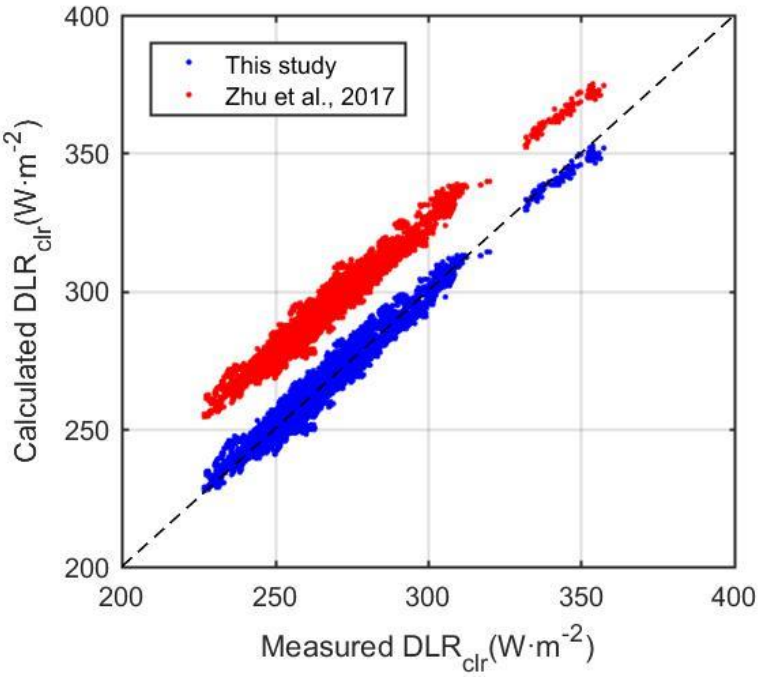

Fig. 3. Scatter plots ofmeasured clear-sky DLR data from as a function of calculations by the Eq.(3) this study (blue dots) and the Eq.(4) by Zhu et al. (2017) (red dots). The dash black line is the 1:1 line.

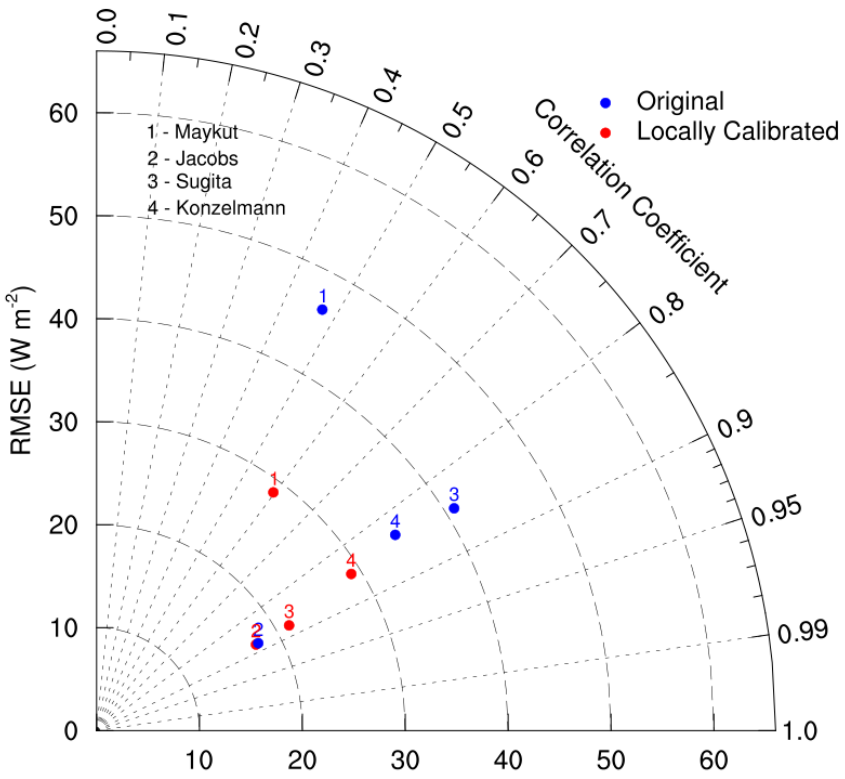

Fig. 4. RMSE and R^2 for the cloudy-sky DLR (DLR_{cld}) parameterizations using the original (blue) and locally calibrated (red) coefficient.

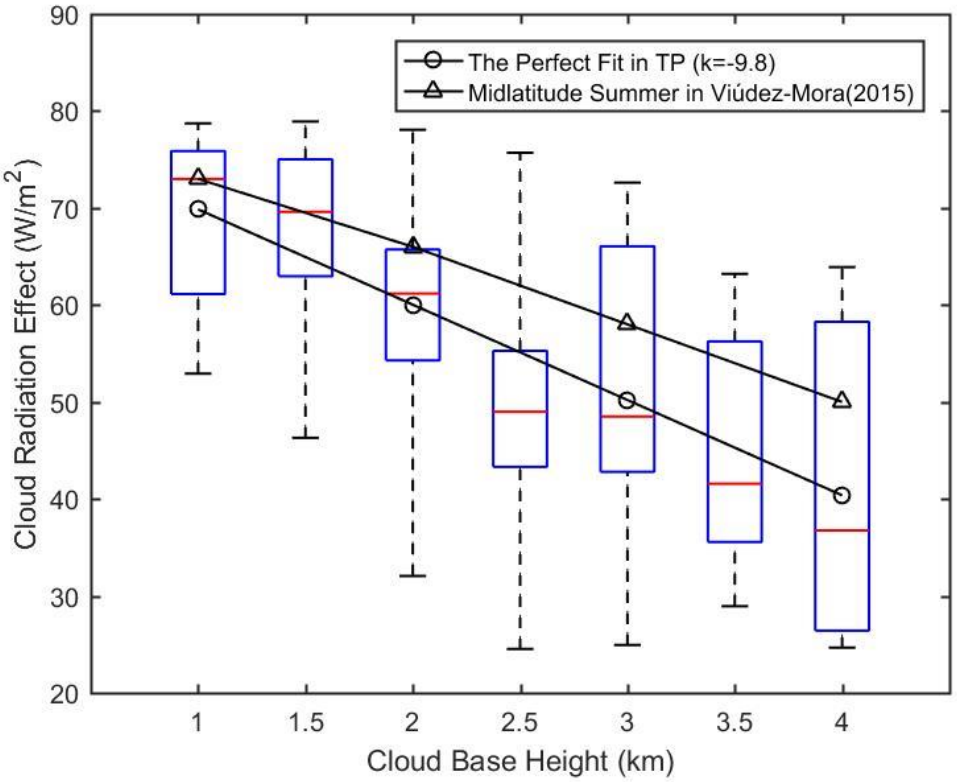

599

600 Fig. 5. Distributions of cloud radiative effect against measured cloud base height are
601 represented by box plot (the blue box indicates the 25th and 75th percentiles, the
602 whiskers indicate 5th and 95th percentiles, the red middle line is the median). The black
603 circles line and the black triangles is mean values of cloud radiative effect over TP in
604 this study and in midlatitude site (Girona, Spain) in Viúdez-Mora(2015) respectively.